Proposal to Jefferson Lab PAC 43

Large Polarization Observables in Wide-angle Compton Scattering at Photon Energies up to 8 GeV

B. Wojtsekhowski (spokesperson-contact), A. Camsonne, P. Degtiarenko,
D. Gaskell, D. Higinbotham, M.K. Jones, C. Keith, C. Keppel, B. Sawatzky, S.A. Wood
Thomas Jefferson National Accelerator Facility, Newport News, VA 23606

S. Abrahamyan (co-spokesperson), A. Asaturyan, A. Mkrtchyan, H. Mkrtchyan,
V. Tadevosyan, A. Shahinyan, H. Voskanyan, S. Zhamkochyan
A.I. Alikhanyan National Science Laboratory, Yerevan 0036, Armenia

G. Niculescu (co-spokesperson), I. Niculescu
James Madison University, Harrisonburg, VA 22807

J. R. M. Annand, D. Hamilton, D. I. Glazier, D. G. Ireland,
K. Livingston, I.J.D. MacGregor, B. McKinnon, B. Seitz, D. Sokhan
University of Glasgow, Glasgow, Scotland

V. Bellini, M. Capogni, E. Cisbani, A. Del Dotto, C. Fanelli, F. Garibaldi,
S. Frullani, F. Mammoliti, G. Salmé, C.M. Sutera, F. Tortorici, G. M. Urciuoli
INFN, Italy

G.B. Franklin, B. Quinn
Carnegie Mellon University, Pittsburgh, PA 15213

A.J.R. Puckett
University of Connecticut, Storrs, CT 06269

A. Ahmidouch and S. Danagoulian
North Carolina A&T State University, Greensboro, NC 27411

G. Cates, R. Lindgren, N. Liyanage, V. Nelyubin
University of Virginia, Charlottesville, VA 22901

The Neutral Particle Spectrometer collaboration:
`https://wiki.jlab.org/cuawiki/index.php/Collaboration`

May 17, 2015

Neutral Particle Spectrometer (NPS) Collaboration

A. Camsonne, R. Ent, P. Nadel-Turoński, S. A. Wood, B. Wojtsekhowski
Jefferson Lab, Newport News, VA 23606

A. Asaturyan, A. Mkrtchyan, H. Mkrtchyan, V. Tadevosyan, S. Zhamkochyan
A.I. Alikhanyan National Science Laboratory, Yerevan 0036, Armenia

M. Guidal, C. Munoz Camacho, R. Paremuzyan
Institut de Physique Nucleaire d'Orsay, IN2P3, BP 1, 91406 Orsay, France

I. Albayrak, M. Carmignotto, J. Dénes-Couto, N. Hlavin, T. Horn, F. Klein, B. Nepal
The Catholic University of America, Washington, DC 20064

C. Hyde, M. N. H. Rashad
Old Dominion University, Norfolk, VA 23529

P. King, J. Roche
Ohio University, Athens, OH 45701

D. Day, D. Keller, O. Rondon
University of Virginia, Charlottesville, VA 22901

D. Hamilton
University of Glasgow, Glasgow, Scotland, UK

S. Širca
University of Ljubljana, Ljubljana, Slovenia

Contents

Abstract

We propose an experiment to measure the initial state helicity correlation asymmetry A_{LL} in Real Compton Scattering (RCS) by scattering circularly polarized photons from a longitudinally polarized proton target at invariant s in the range of 8 to 16 GeV^2 for several scattering angles between $\theta_p^{\rm cm} = 80^\circ$ and $\theta_p^{\rm cm} = 100^\circ$.

Two JLab RCS experiments, E99-114 and E07-002, have demonstrated the feasibility of the experimental real Compton scattering technique at JLab using an untagged photon beam of high intensity and have provided high accuracy results for the cross section and polarization parameter K_{LL}, admittedly at relatively low values of $s, -t, -u$ for K_{LL}. In the 6 GeV era there was an approved A-rated JLab experiment (E-05-101) to measure A_{LL} which did not get beam time due to a schedule problem and polarized target failure. PAC42 recently supported experiment E12-14-006, which has a similar scope. The analysis completed in January 2015 of the E07-002 experiment shows an unexpected result for the polarization transfer parameter K_{LL}, which was found to be 3 times larger than predicted by the GPD-based model at $\theta_p^{\rm cm} = 70^\circ$.

Such news motivates this proposed study of the polarization effect in WACS at significantly higher s than was done (or proposed) before. Our experiment utilizes an untagged bremsstrahlung photon beam and the polarized target used in the *g2p* experiment with the target field oriented along the beam direction. The scattered photon will be detected in the Neutral Particle Spectrometer (NPS), while the coincident recoil proton will be detected in the Super BigBite Spectrometer (SBS). An intense photon beam will be produced at a distance of 2 m from the target and cleaned from an electron beam by means of a shielded magnet-dump.

The applicability of QCD, in the medium energy range, to exclusive reactions is a subject of great interest, and any opportunity to unambiguously test its predictions should be taken. This proposal's experimental setup has a figure-of-merit (FOM) 100x larger than known polarized target RCS experiments, and it will carry out its measurements at large s (8-16 GeV^2) and $-t$ (3-7 GeV^2). These are optimal conditions for testing the applicability domain of GPDs and addressing the (apparent) puzzles listed above.

We request 350 hours of an electron beam with 1.2 μA at 8.8 GeV energy to measure the polarization observable A_{LL} to a statistical accuracy better than 0.09 in a wide-angle regime near $\theta_p^{\rm cm} = 90^\circ$ at four values of s. This measurement will significantly increase our experimental confidence in the application of the GPD approach to reactions induced by real photons, which will play a major role in nucleon structure physics at JLab.

1 Physics Motivation

Understanding the structure of hadrons in terms of QCD is one of the fundamental goals of modern nuclear physics. The formalism of Generalized Parton Distributions (GPD) developed about 20 years ago for the first time linked hadron structure information accessible through inclusive reactions such as Deep Inelastic Scattering (DIS) to information from exclusive reactions. These GPDs, while not directly measurable in experiments, provide a unified description of key electromagnetic reactions on the nucleon [1]. Whereas DIS allows investigation of the longitudinal structure of the nucleon, exclusive reactions such as elastic electron and photon scattering access its transverse structure. Taken together they allow determination of a complete image of the nucleon and its complex substructure [2].

Wide Angle Compton Scattering (WACS) from the nucleon with large values of s, $-t$, and $-u$ compared with Λ^2_{QCD} is a hard exclusive process which provides access to information about nucleon structure that is complementary to high Q^2 elastic form factors and Deeply Virtual Compton Scattering. The common feature of these reactions is a large energy scale, leading to factorization of the scattering amplitude into a hard perturbative kernel and a factor described by soft non-perturbative wave functions.

Various theoretical approaches have been applied to WACS in the hard scattering regime, and these can be distinguished by the number of active quarks participating in the hard-scattering subprocess, or equivalently, by the mechanism for sharing the transferred momentum among the constituents. Two extreme pictures have been proposed. In the perturbative QCD (pQCD) approach, three active quarks share the transferred momentum by the exchange of two hard gluons [3, 4]. In the handbag approach, which has in recent years become a staple in the interpretation of data from hard exclusive reactions, only one quark is assumed to be active, whose wave function has sufficient high-momentum components for the quark to absorb and re-emit the photon [5, 6, 7]. In any given kinematic regime both mechanisms will contribute, in principle, to the cross section. It is generally believed that, at sufficiently high energies, the pQCD mechanism dominates. However, in the currently accessible experimental domain of s and t, the nature of the reaction mechanism is not fully understood.

Three other theoretical advances based on leading-quark dominance in WACS have been proposed in recent years. The constituent quark model with a handbag diagram has proven successful in describing the WACS process [8], as have calculations performed in a generalized Vector Meson Dominance (VMD) framework [9]. More recently, the soft-collinear effective theory (SCET) was developed for elastic electron-proton scattering at high momentum transfer [10]. The QCD factorization approach formulated in the framework of SCET allows the development of a description of the soft-spectator scattering contribution to the overall amplitude. The two-photon exchange (TPE) contributions to elastic electron-proton scattering were shown to factorize by the introduction of a single, universal SCET form-factor which defines the dominant soft-spectator amplitudes. As the same form factor also naturally arises in wide-angle Compton scattering, it is argued in Refs. [10] that the most promising route for understanding this soft spectator contribution in hard exclusive reactions at JLab energies is through the study of WACS.

One of the main predictions of the pQCD mechanism for WACS is the constituent scaling

rule [11], whereby $d\sigma/dt$ scales as s^{-6} at fixed θ_{cm}. The pioneering experiment at Cornell [12] was approximately consistent with constituent scaling, albeit with modest statistical precision. However, the high-precision data from JLab gave a scaling power of $s^{-7.5\pm0.2}$ [13]. The calculations from both the GPD-based handbag approach and the SCET framework have reproduced the JLab cross section data very well. Crucially, the extracted values of the SCET form factor do not show any significant dependence on the value of s as required by factorization, in agreement with [10]. The polarization transfer observables were previously measured at JLab for Compton scattering at $s = 6.9$ and $t = -4.1$ GeV^2 in experiment E99-114 [14]. It was found that the longitudinal component of the polarization transfer at this kinematic point is large and positive in agreement with the handbag GPD and SCET predictions, and in unambiguous disagreement with the pQCD predictions.

In view of the remarks above, we consider several interesting questions that motivate us to explore further the measurement of polarization observables in WACS at JLab:

1. What is the nature of the quark which absorbs and emits photons in the WACS process in the wide angle regime? Is it a constituent or a current quark?

2. What is the energy scale at which the GPD mechanism becomes dominant? This experiment will explore this question at large s, 8-16 GeV^2, and $-t$, 3-7 GeV^2.

3. If the GPD approach is correct, is it indeed true that the WACS reaction proceeds through the interaction of photons with a single quark?

4. What are the constraints on the GPD integrals imposed from the proposed measurement of the A_{LL} observable?

5. What is the role of a diquark *ud* correlation in WACS?

In order to present a framework for addressing these issues, we next briefly discuss WACS in the soft-collinear effective theory, the handbag mechanism in the GPD conceptualization, and the handbag mechanism in the constituent quark model.

1.1 Soft-collinear Effective Theory

Recent theoretical developments have led to a complete factorization of the leading power contribution in Wide-angle Compton scattering [10, 15, 16]. The soft-spectator contribution describes the scattering which involves the soft modes and resulting soft-spectator scattering contribution to the overall amplitude. The soft collinear effective theory is used in order to define this contribution in a field theoretical approach. The SCET framework is then used to provide a proof of the factorization formula.

The SCET framework permits the implementation of some specific corrections which are related to the soft-overlap contribution. There are indications that a numerical effect of this contribution can be dominant at some moderate values of the Mandelstam variables. In general, SCET gives a very solid description in the region where the other power corrections are small.

The SCET formalism follows the same idea as in the standard factorization approach; Short and long distance physics are factorized separately. The only required assumptions are very general such as that soft partons have soft momenta on the order of Λ_{qcd}. There is no additional need to constrain the virtualities by hand. The advantage of SCET formalism is a systematic approach to the factorization of the hard and soft subprocesses.

The asymmetry K_{LL} is studied with the assumption that the hard-spectator contributions are small. Neglecting all power corrections and using the next-to-leading expressions, some numerical results as a function of the scattering angle θ are obtained (see Fig. 1). The solid red line corresponds to the leading-order approximation. The dashed (blue) and dotted (black) lines show the numerical results for the complete NLO expression for the energies $s = 6.9$ GeV^2 and s=20 GeV^2, respectively. The data point is from E99-114 and corresponds to s=6.9 GeV^2. The value of the longitudinal asymmetry K_{LL} is qualitatively different from the one that can be obtained in the hard-spectator (hard two-gluon exchange) factorization picture.

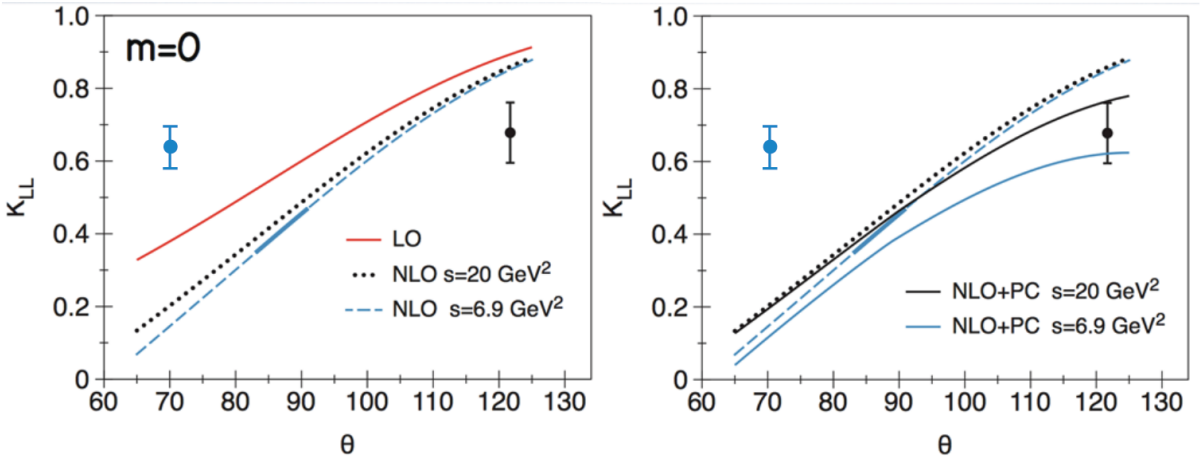

Figure 1: The longitudinal asymmetry K_{LL} as a function of scattering angle θ. (Left) A comparison of the LO (red) and NLO calculated with s=6.9 GeV^2(dashed) and s=20 GeV^2 (dotted) lines. (Right) A comparison of the NLO results calculated with (solid black) and without (solid blue) kinematical power corrections. The massless approximation is the same for both plots [15].

It is very relevant to describe a factorization for the helicity flip amplitudes, but the modeling will be dependent on the new unknown nonperturbative matrix elements. Any experimental data on A_{LL} directly can provide the needed information to move forward in the acquisition of these nonperturbative quantities.

1.2 pQCD Mechanism

The traditional framework for the interpretation of hard exclusive reactions in the asymptotic regime is perturbative QCD (pQCD) [17, 18]. The onset of scaling in Deep Inelastic Scattering (DIS) at the relatively low scale of Q^2 ~1 - 2 GeV^2 gives rise to the expectation that pQCD might also be applicable to exclusive processes in the range of a few GeV^2. pQCD confronts WACS [3, 4, 19] as shown in Fig. 2, where it is seen that the three valence quarks

are active participants in the hard subprocess, which is mediated by the exchange of two hard gluons. The soft physics is contained in the valence quark distribution amplitudes. The pQCD mechanism leads naturally to the constituent counting rules for exclusive processes:

$$\frac{d\sigma}{dt} = \frac{f(\theta_{cm})}{s^n}, \quad (1)$$

where n is related to the number of active constituents in the reaction and $f(\theta_{cm})$ is a function only of the center of mass scattering angle [11, 20]. Indeed, the observation that many exclusive reactions, such as elastic electron scattering, single-pion photoproduction, and WACS, approximately obey Eq. 1 has led to the belief that the pQCD mechanism dominates at experimentally accessible energies. There seems to be little theoretical disagreement that the pQCD mechanism dominates at sufficiently high energies [17]; however, there is no consensus on How high is "sufficiently high"? Despite the observed scaling, absolute cross sections calculated using the pQCD framework are very often low compared with existing experimental data, sometimes by more than an order of magnitude [19, 21].

Moreover, several recent precision JLab experiments that measure polarization observables also disagree with the pQCD. In the G_E^p experiment [22, 23, 24], the slow falloff of the Pauli form factor $F_2(Q^2)$ up to Q^2 of 8.5 GeV^2 provides direct evidence that hadron helicity is not conserved, contrary to predictions of pQCD. Similar findings were made in the π^0 photoproduction experiment [25], where both the non-zero transverse and normal components of polarization of the recoil proton are indicative of hadron helicity-flip, which is again contrary to the predictions of pQCD. Finally, in the WACS experiment E99-114 and new data available from E07-002, the longitudinal polarization transfer K_{LL} (which will be defined precisely in the next section) shows a value which is large and positive, contrary to the pQCD prediction which is small and negative [19]. For all these reasons, it can be argued that pQCD is not the correct mechanism for interpreting exclusive reactions at currently accessible energies and instead we should seek a description in terms of the handbag mechanism. The pQCD calculations predict that A_{LL}=K_{LL}, so a measurement of A_{LL} in combination with the already obtained result for K_{LL} could provide an additional test of pQCD applicability in the JLab energy regime.

1.3 Handbag Mechanism

The handbag mechanism offers new possibilities for the interpretation of hard exclusive reactions. For example, it provides the framework for the interpretation of deep exclusive reactions, which are reactions initiated by a high-Q^2 virtual photon. The application of the formalism to WACS (see Fig. 3) was initially worked out to leading order (LO) by Radyushkin [5] and subsequently by Diehl *et al.* [6]. The next-to-leading-order (NLO) contributions have been worked out by Huang *et al.* [7]. The corresponding diagram for elastic electron scattering is similar to Fig. 3, except that there is only one external virtual photon rather than two real photons. In the handbag approach, the hard physics is contained in the scattering from a single active quark and is calculable using pQCD and QED: It is just Compton scattering from a structureless spin-1/2 particle.

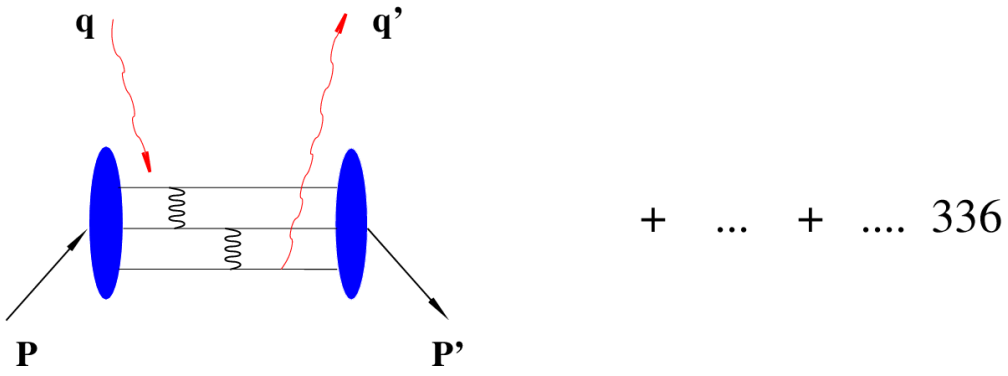

Figure 2: Two gluon exchange pQCD diagram for WACS. A total of 336 different diagrams contribute.

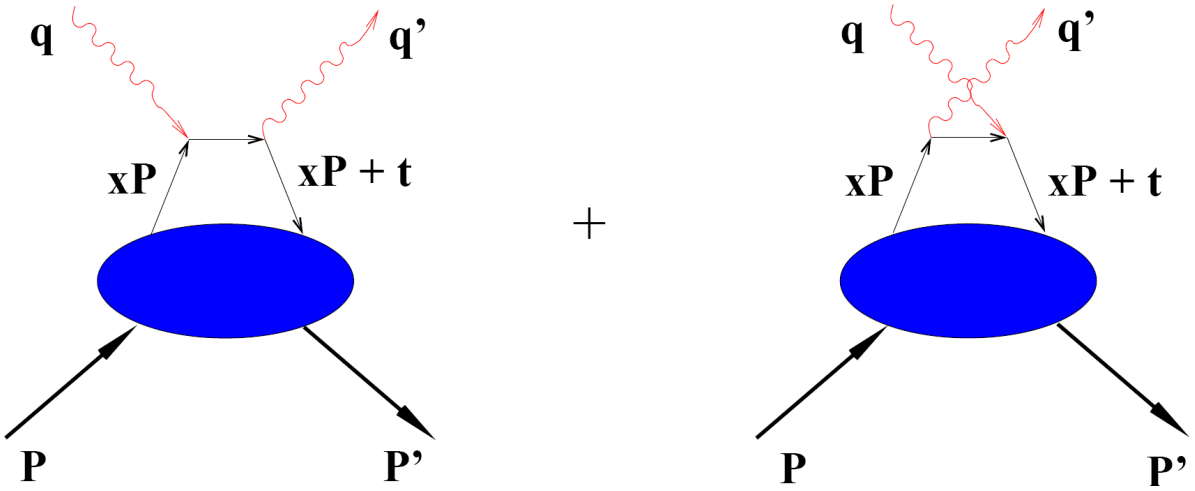

Figure 3: The handbag diagram for WACS.

The soft physics is contained in the wave function describing how the active quark couples to the proton. This coupling is described in terms of GPDs. The GPDs have been the subject of intense experimental and theoretical activity [26, 27]. They represent "superstructures" of the proton, from which are derived other measurable structure functions, such as parton distribution functions (PDF) and form factors (F_1 and F_2). To NLO, only three of the four GPDs contribute to the WACS process: $H(x,\xi=0,t)$, $\hat{H}(x,\xi=0,t)$, and $E(x,\xi=0,t)$. Since the photons are both real, the skewness parameter ξ is zero, reflecting the fact that the momentum absorbed by the struck quark is purely transverse. In the handbag formalism, the WACS observables are new form factors of the proton that are x^{-1}-moments of the GPDs:

$$R_{_V}(t) \;=\; \sum_a e_a^2 \int_{-1}^{1} \frac{dx}{x} H^a(x,0,t),$$

$$
\begin{aligned}
R_{_A}(t) &= \sum_a e_a^2 \int_{-1}^{1} \frac{dx}{x} \,\mathrm{sign}(x)\, \hat{H}^a(x,0,t), \\
R_{_T}(t) &= \sum_a e_a^2 \int_{-1}^{1} \frac{dx}{x} E^a(x,0,t),
\end{aligned}
$$

where e_a is the charge of the active quark and the three form factors are, respectively, the vector, axial vector, and tensor form factors. ($\mathrm{sign}(x)$ is the sign of x $\equiv \frac{x}{|x|}$.) The corresponding form factors for elastic electron or neutrino scattering are given by the first (x^0) moments of the same GPDs:

$$
\begin{aligned}
F_{_1}(t) &= \sum_a e_a \int_{-1}^{1} dx\, H^a(x,0,t), \\
G_{_A}(t) &= \sum_a \int_{-1}^{1} dx\, \mathrm{sign}(x)\, \hat{H}^a(x,0,t), \\
F_{_2}(t) &= \sum_a e_a \int_{-1}^{1} dx\, E^a(x,0,t),
\end{aligned}
$$

where the three quantities are, respectively, the Dirac, axial, and Pauli form factors. On the other hand, the $t = 0$ limit of the GPDs produce the PDFs:

$$
\begin{aligned}
H^a(x,0,0) &= q^a(x), \\
\hat{H}^a(x,0,0) &= \Delta q^a(x) \\
E^a(x,0,0) &= 2\frac{J^a(x)}{x} - q^a(x),
\end{aligned} \tag{2}
$$

where J^a is the total angular momentum of a quark of flavor a and is not directly measurable in DIS.

In the handbag factorization scheme, the WACS helicity amplitudes are related to the form factors by

$$
\begin{aligned}
M_{\mu'+,\mu+}(s,t) &= 2\pi\alpha_{em} \left[T_{\mu'+,\mu+}(s,t)(R_{_V}(t) + R_{_A}(t)) + T_{\mu'-,\mu-}(s,t)(R_{_V}(t) - R_{_A}(t)) \right], \\
M_{\mu'-,\mu+}(s,t) &= 2\pi\alpha_{em} \frac{\sqrt{-t}}{m} \left[T_{\mu'+,\mu+}(s,t) + T_{\mu'-,\mu-}(s,t) \right] R_{_T}(t),
\end{aligned}
$$

where μ, μ' denote the helicity of the incoming and outgoing photons, respectively. The signs on M and T refer to the helicities of the proton and active quark, respectively. This structure of the helicity amplitudes leads to a simple interpretation of the WACS form factors: $R_{_V} \pm R_{_A}$ is the response of the proton to the emission and reabsorption of quarks with helicity in the same/opposite direction of the proton helicity, and $R_{_T}$ is directly related to the proton helicity-flip amplitude [7]. These equations lead to expressions relating WACS observables to the form factors.

The most important of these experimentally are the spin-averaged cross section, the recoil polarization observables and $A_{_{LL}}$. The spin-averaged cross section factorizes into a simple

product of the Klein-Nishina (KN) cross section describing the hard scattering from a single quark, and a sum of form factors depending only on t [5, 6]:

$$\frac{d\sigma/dt}{d\sigma_{\rm KN}/dt} = f_{_V}\left[R_{_V}^2(t) + \frac{-t}{4m^2}R_{_T}^2(t)\right] + (1-f_{_V})R_{_A}^2(t)\,. \tag{3}$$

For the interesting region of large $p_\perp$, the kinematic factor $f_{_V}$ is always close to 1. Consequently the unpolarized cross sections are largely insensitive to $R_{_A}$, and the left-hand side of Eq. 3 is nearly s-independent at fixed t. One of the primary goals of E99-114 was to test this relationship as well as to determine the vector form factor $R_{_V}$. Calculations to NLO, which take into account both photon and proton helicity-flip amplitudes, do not change this prediction in any appreciable way [7, 28]. Updated cross section and Compton form factors (see Fig. 4) with their parametric uncertainties have also been evaluated [29].

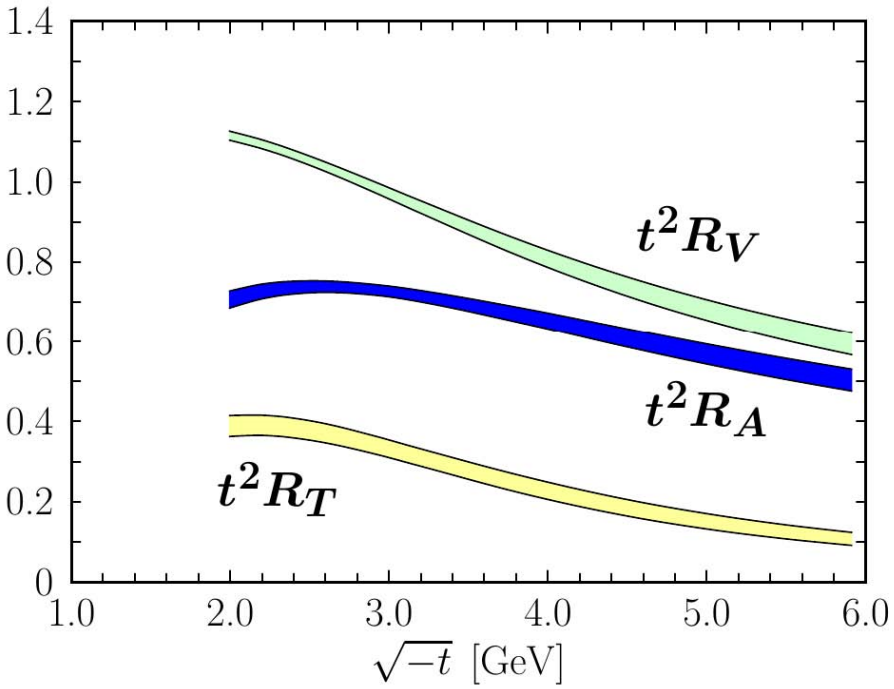

Figure 4: Predictions for the Compton form factors evaluated from the M. Diehl, P. Kroll default fit from Ref. [7], scaled by t^2 and shown in units of GeV^4. The bands in each case show the parametric uncertainties.

The longitudinal and transverse polarization transfer observables, $K_{_{LL}}$ and $K_{_{LS}}$, respectively, are defined by

$$K_{_{LL}}\frac{d\sigma}{dt} \equiv \frac{1}{2}\left[\frac{d\sigma(\uparrow\uparrow)}{dt} - \frac{d\sigma((\downarrow\uparrow)}{dt}\right] \qquad K_{_{LS}}\frac{d\sigma}{dt} \equiv \frac{1}{2}\left[\frac{d\sigma(\uparrow\rightarrow)}{dt} - \frac{d\sigma(\downarrow\rightarrow)}{dt}\right] \tag{4}$$

where the first arrow refers to the incident photon helicity and the second to the recoil proton helicity ($\uparrow$) or transverse polarization ($\rightarrow$).

With definitions of two additional parameters,

$$\beta \;=\; \frac{2m}{\sqrt{s}}\,\frac{\sqrt{-t}}{\sqrt{s}+\sqrt{-u}} \qquad \kappa(t) \;=\; \frac{\sqrt{-t}}{2m}\,\frac{R_{_T}(t)}{R_{_V}(t)}\,, \tag{5}$$

the three polarization observables are approximately related to the form factors by the expressions [6, 7],

$$K_{_{LL}} \;\approx\; K_{_{LL}}^{\rm KN}\,\frac{R_{_A}(t)}{R_{_V}(t)}\,\frac{1-\beta\kappa(t)}{1+\kappa^2(t)} \qquad \frac{K_{_{LS}}}{K_{_{LL}}} \;\approx\; \kappa(t)\,\frac{1+\beta\kappa^{-1}(t)}{1-\beta\kappa(t)} \qquad P_{_N} \;\approx 0\,, \tag{6}$$

where $K_{_{LL}}^{\rm KN}$ is the longitudinal asymmetry for a structureless Dirac particle. These formulas do not include small gluonic corrections, which are discussed in Ref. [7].

The expressions above show that measurements of $K_{_{LL}}$ and $K_{_{LS}}$, when combined with measurements of $d\sigma/dt$, allow determinations of all three form factors. They also show that two very important pieces of information follow directly from the spin asymmetries: $K_{_{LL}}$ and $K_{_{LS}}$ / $K_{_{LL}}$, which are directly related to the form factor ratios $R_{_A}/R_{_V}$ and $R_{_T}/R_{_V}$, respectively.

The initial state helicity correlation parameter is defined by,

$$A_{_{LL}}\frac{d\sigma}{dt} \;\equiv\; \frac{1}{2}\left[\frac{d\sigma(\uparrow\uparrow)}{dt} - \frac{d\sigma((\downarrow\uparrow)}{dt}\right], \tag{7}$$

where the first arrow refers to the incident photon helicity and the second to the initial state proton helicity ($\uparrow$). In the GPD approach of Ref. [7], the initial state helicity correlation parameter, $A_{_{LL}}$, equals $K_{_{LL}}$ so all the predicted relationships between $A_{_{LL}}$ and the WACS form factors are the same as shown above for $K_{_{LL}}$.

From the relationships (Eq. 2) connecting the WACS form factors to PDFs, the ratio $R_{_A}/R_{_V}$ is related to $\Delta q^a(x)/q^a(x)$. For WACS, the e_a^2-weighting of the quark flavors means that u quarks will dominate the reaction. Moreover, at relatively large $-t$, the contributions to the form-factor integral are concentrated at moderate-to-high x, where the valence quarks dominate. Therefore, the $A_{_{LL}}$ asymmetry contains direct information on $\Delta u(x)/u(x)$ in the valence region. We propose to investigate this in the present experiment, up to $-t = 5.4$ GeV^2.

Obtaining this kind of information is one of the key physics elements justifying the 12 GeV upgrade of JLab. From the correspondence between WACS and electron scattering form factors, there is expected to be a close relationship between $R_{_T}/R_{_V}$ and F_2/F_1 [7]. The measurements of G_E^p at JLab [22, 23, 24] have shown that F_2/F_1 falls as $1/\sqrt{-t}$ rather than as $1/t$, the latter being predicted by pQCD. It will be an important check on the theoretical interpretation of $F_{_2}/F_{_1}$ to see if $R_{_T}/R_{_V}$ behaves in a similar way. The results from E99-114 at $-t = 4$ are large but suggest that the $R_{_T}/R_{_V}$may fall more rapidly with $-t$ than $F_{_2}/F_{_1}$. Experiment E07-002 is expected to obtain better precision on K_{LT} and $K_{_{LL}}$ leading to new results for the relationship between $F_{_2}/F_{_1}$ and $R_{_T}/R_{_V}$. In fact, E07-002 got an unexpected result for $K_{_{LL}}$, which put primary interest in verification of the reraction mechanism by the measurement at higher s.

1.4 Relativistic constituent quark model for WACS

The relativistic constituent quark model developed by G.A. Miller [8] addresses the question of what the dominant reaction mechanism is that allows the proton to accommodate the large momentum transfer in exclusive reactions such as elastic electron and photon scattering. This model has been successful in describing the electromagnetic nucleon form factors [30]. Unlike the handbag calculations within the GPD approach [6, 7], Miller's model does not neglect quark and hadron helicity flip. The model starts with a wave function for three relativistic constituent quarks:

$$\Psi(p_i) = u(p_1)u(p_2)u(p_3)\psi(p_1, p_2, p_3),$$

where p_i represents space, spin, and isospin indices. It evaluates the wave function in the light cone variables and the calculations are relativistic. They obey gauge invariance, parity conservation, and time reversal invariance. They include quark mass effects and proton helicity flip. Due to lower components of Dirac spinors, where the quark spin is opposite to that of the proton, quark orbital angular momentum appears. The resulting predictions for the polarization observables A_{LL} and K_{LL} and the cross section are shown in Fig. 5 and Fig. 6, together with data from the E99-114 experiment. The most striking consequence of Miller's results is a big difference between A_{LL} and K_{LL} at large scattering angles, which we can test experimentally.

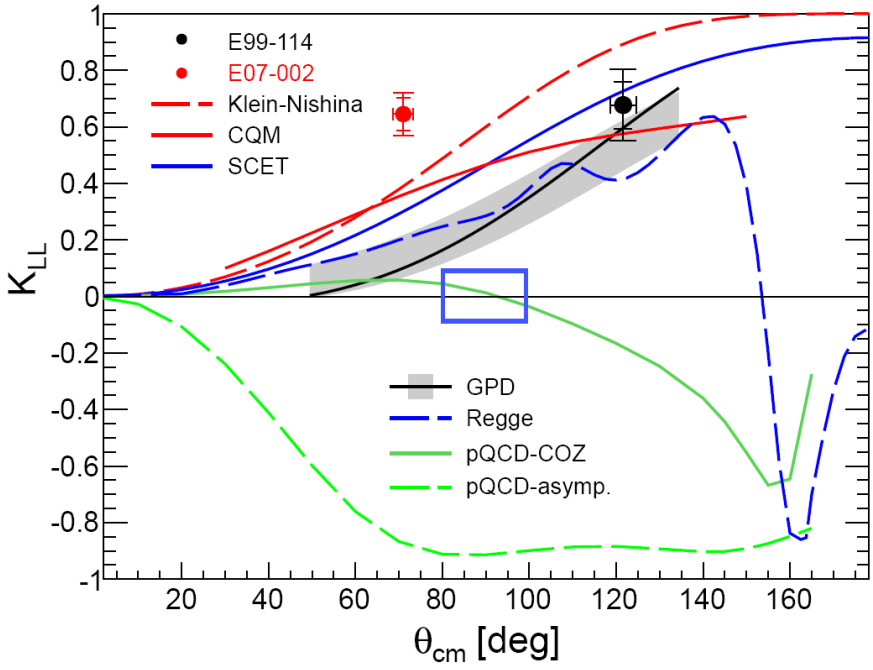

Figure 5: Predictions for A_{LL} in the GPD approach of Ref. [7] and CQM of Ref. [8] along with the data on K_{LL} from E99-114 and E07-002 and the expected range and precision of the proposed measurements (blue box).

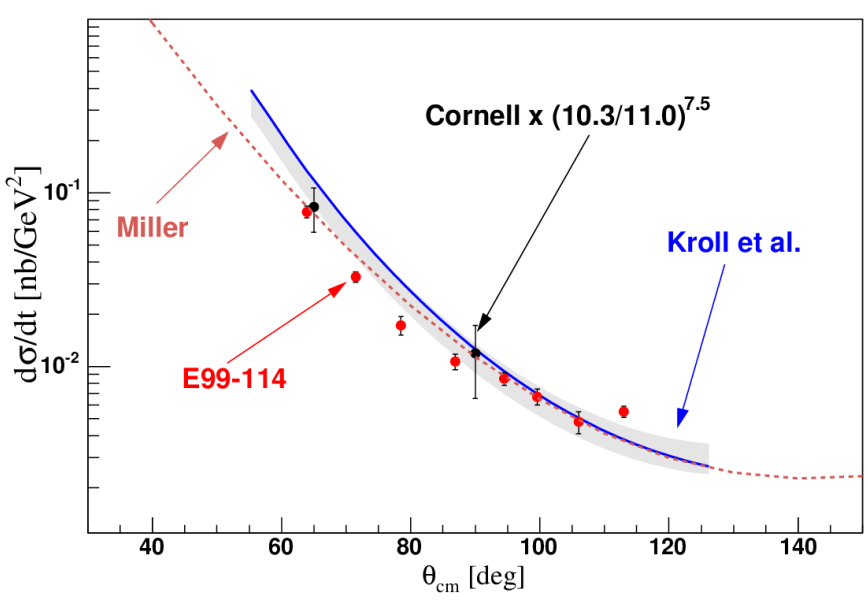

Figure 6: Cross section of WACS process at s = 11 GeV^2 from E99-114 and Cornell[12] experiments (scaled to the same CM energy) and results of calculations in the GPD approach (Kroll) and from a CQM (Miller).

1.5 Polarization observables in QED Compton process

It is instructive to evaluate polarization effects in the QED process $e\gamma \to e\gamma$. The Klein-Nishina process is an example that is fully calculable and which plays a major role in WACS, when the handbag diagram dominates. It is useful to evaluate polarization observables for different ratios of the electron mass to the photon energy.

Polarization observables in QED are given in invariant variables as [31] :

$$A_{LL}^{KN} = \left[-\frac{s-m^2}{u-m^2} + \frac{u-m^2}{s-m^2} - \frac{2m^2t^2(s-u)}{(s-m^2)^2(u-m^2)^2}\right] / \left[-\frac{s-m^2}{u-m^2} - \frac{u-m^2}{s-m^2} + \frac{4m^2t(m^4-su)}{(s-m^2)^2(u-m^2)^2}\right]$$

$$K_{LL}^{KN} = \left[-\frac{s-m^2}{u-m^2} + \frac{u-m^2}{s-m^2} - \frac{4m^2t^2(m^4-su)}{(s-m^2)^3(u-m^2)^2}\right] / \left[-\frac{s-m^2}{u-m^2} - \frac{u-m^2}{s-m^2} + \frac{4m^2t(m^4-su)}{(s-m^2)^2(u-m^2)^2}\right]$$

Figure 7 shows the A_{LL}^{KN} and K_{LL}^{KN} for different energies of the incident photon as a function of the scattering angle in the electron rest frame. At low t/s and for $m/E_\gamma << 1$ the difference between K_{LL} and A_{LL} vanishes. At $\theta_{lab} = \pi/2$ the observable A_{LL}=0. In the limit $m/E_\gamma \to 0$ A_{LL}=K_{LL} for all values of θ_γ not equal to 180°. At $\theta_\gamma = 180°$ the value of $A_{LL} \approx -K_{LL}$. In Miller's calculation (see Figure 5), which has $m/E_\gamma \sim 1/10$ and $\theta_{lab} \approx 90°$, the difference between K_{LL} and A_{LL} is about 0.7.

1.6 Additional Remarks

It is important to realize that the issues posed at the start of this section are not limited to the WACS reaction. Single-pion photoproduction and deuteron photo–disintegration pose

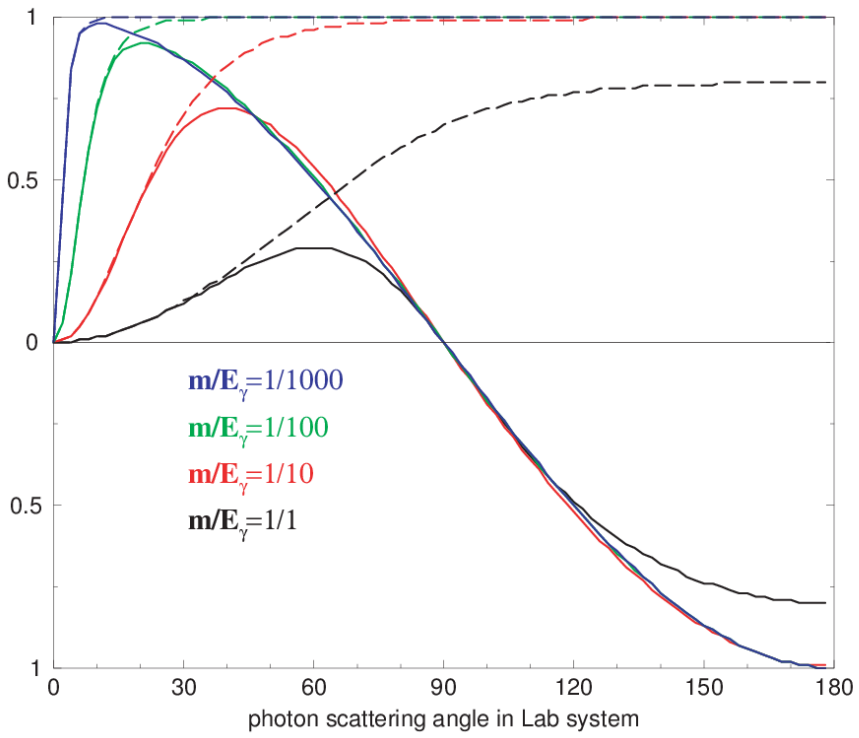

Figure 7: Klein-Nishina polarization observables A_{LL} and K_{LL}, shown by solid lines and dashed lines respectively, for different ratios of the electron mass to the photon energy as a function of the scattering angle in the lab system.

similar problems. Indeed, they are questions that need to be addressed by all studies of the proton using exclusive reactions in the hard scattering regime. While reaction mechanisms at a few GeV^2 are not simple, it is precisely their non–triviality that makes them a fertile ground for testing competing theoretical approaches.

The old paradigm for addressing these questions was the pQCD mechanism and the distribution amplitudes. It is quite likely that the new paradigm will be the handbag mechanism and GPDs. Mapping out in what region of s and t the handbag diagram is/becomes dominant will be a tremendous achievement for our field. In any case, the reaction mechanism needs to be tested, not only over a wide range of kinematic variables but also over a wide range of different reactions. Of these, WACS offers the simplest/best possibility to test the mechanism free of complications from additional hadrons. To date, the CQM has been quite successful in describing many of the observables of the hadronic structure and in painting a useful and intuitive picture of the hadron. This proposal will examine, with good precision, a unique regime/case where predictions of the CQM and QCD–based theory are qualitatively different.

1.7 Summary of Physics Goals

We propose measurements of the spin correlation asymmetry A_{LL} for incident photon energies up to 8 GeV (s =8 to 16 GeV^2) for several scattering angles between $\theta_p^{\rm cm} = 80^\circ$ and $\theta_p^{\rm cm} = 100^\circ$ (corresponding to $-t$ =3.0-7.0 GeV^2). The specific physics goals are as follows:

1. To make a measurement of A_{LL} at largest possible s, t and u where one expects the applicability of GPD-based calculations to be under control. A high precision measurement is likely to resolve the discrepancy between the surprising results from experiment E07-002 and the GPD predictions which are in reasonable agreement with Hall A measurements.

2. To provide a test that can expose, in an unambiguous way, how the WACS reaction proceeds: either via the interaction of photons with a current quark, or with a constituent quark.

3. To extract the form factor ratio R_A/R_V from the measurement of A_{LL} and correlate this result with the F_2/F_1 ratio determined from elastic electron scattering.

The overall statistical precision with which we will address these physics goals will be discussed in Sec. 5.

2 Experimental Setup

The proposed experiment will study the scattering of polarized photons from a polarized hydrogen target, as illustrated in Fig. 8. The scattered photon will be detected by the Neutral Particle Spectrometer (NPS) positioned at 28° and installed at a distance of 2 m from the target to match the acceptance of the SBS (which will be used to detect the recoiling proton), positioned at 25°, 3.7 m from the target. The Photon Source combines a 10% radiator with a normal conducting, heavily shielded magnet that sweeps away primary beam electrons, producing a narrow (0.9 mm diameter on target) untagged photon beam. The distance between the radiator and the target will be 2 m. This device is described in detail in Section 3.

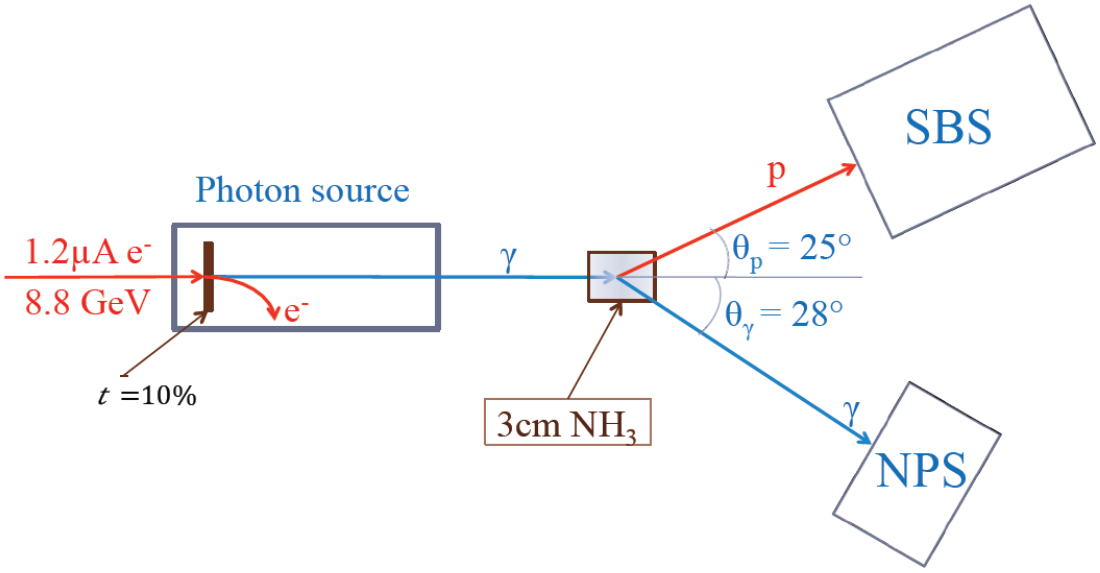

Figure 8: Schematic of the experimental setup. The target is longitudinally polarized (along the beam). The scattered photon is detected by the NPS and the recoil proton is detected by the SBS. The photon source provides a narrow, 0.9 mm diameter on target, untagged bremsstrahlung photon beam.

We plan to use an incident electron beam of 8.8 GeV with intensity of 1.20 μA and 80% polarization. Such currents are large enough to enable precision beam measurements ensuring stable, quality primary beam delivery. Using the magnet sweeper/dump combination and the radiator produces a narrow photon beam. Our calculations put the heat load on the beam on the polarized target a factor of 30-40 times lower than a corresponding mixed-beam of similar intensity (see Sec. 2.1).

The target will be a longitudinally polarized proton, similar to the target successfully used for the $g2p$ experiment [32] (experiments E08-027/E08-007), operating in a 5 Tesla field pointing along the beam line (longitudinal).

We expect this target to match the average NH_3 polarization of 75% achieved in several 6

GeV-era experiments: RSS and SANE experiments in Hall C, $g2p$ and G_E^p experiments in Hall A. The beam polarization will be measured (using a Möller polarimeter) with a systematic uncertainty of 2%. The large cross section and helicity asymmetry for π^0 photoproduction, as determined in E99-114, will provide a monitor of the electron beam polarization continuously during data taking at fixed kinematic conditions with large $\theta_p^{\rm cm}$, see discussion in Sec. 4.2 on signal extraction.

2.1 The Polarized Hydrogen Target and the Radiator

In this experiment we will use the $g2p$ polarized target previously used in the 6 GeV-era. A schematic of this target is shown in Figure 9. The target will be polarized in the longitudinal direction.

This target operates on the principle of Dynamic Nuclear Polarization (DNP). The low temperature (1 K°), high magnetic field (5 T) natural polarization of solid materials (ammonia, lithium hydrides) is enhanced by microwave pumping. The polarized target assembly contains two 3–cm–long target cells that can be selected individually by remote control to be located in the uniform field region of a superconducting Helmholtz pair. There are also two other target cells which are available for a calibration target like carbon foil or CH_2. The permeable target cells are immersed in a vessel filled with liquid helium and maintained at 1 K by the use of a high power evaporation refrigerator. The magnet coils have a 55° conicaly shaped aperture along the axis and a 38° wedge shaped aperture along the vertically oriented midplane.

The target material, during the experiment, will be exposed to 140 GHz microwaves to drive the hyperfine transition which aligns the nucleon spins. The DNP technique produces proton polarizations of up to 95% in the NH_3 target. The heating of the target by the beam causes an initial drop of a few percent in the polarization. Then the polarization slowly decreases due to radiation damage. Most of the radiation damage is repaired by annealing the target at about 80° K, until the accumulated dose reaches $> 2\times10^{17}$ per cm^2 electrons, at which point the material needs to be changed. Due to limitations in the heat removal by the refrigerator, the electron beam intensity on the target is limited to 90 nA. The heat load on the target with pure photon beam is mainly due to photo production of the electron-positron pairs in the target materials. The effective beam intensity on target I_{eff} could be calculated as follows:

$$I_{eff} \;=\; I_e \times t_r \times \frac{7}{9} t_t \times \ln E_{max}/E_{min} \;=\; I_e \times 0.022, \tag{8}$$

where I_e is electron beam intensity on the radiator, $t_r = 0.1$ is the radiator thickness in units of radiation length, $t_t = 0.03$ is the target thickness in units of radiation length, $E_{max} = 8800$ MeV is the maximum energy of the photon, and $E_{min} \approx 5$ MeV is a critical energy above which the photon interaction is dominated by pair production in material of the target. Taking into account the material of the target cap, we estimate that $I_{eff} \approx 0.025 - 0.33\, I_e$. For the proposed beam on the radiator of 1200 nA, the effective beam on the target is 30-40 nA. At such intensity the target annealing needs to be performed only one time during the run and target polarization could be maintained close to 85%.

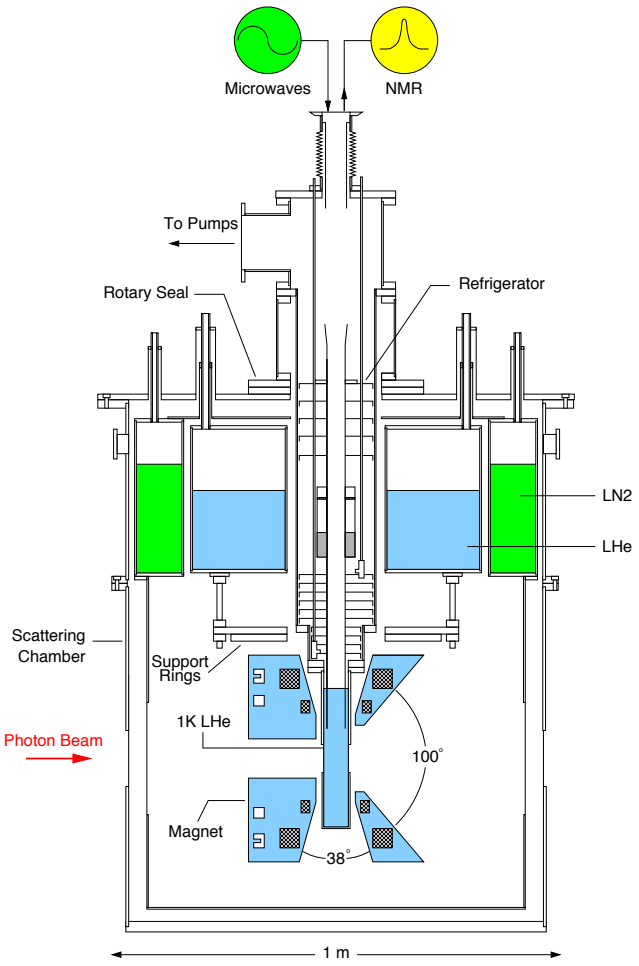

Figure 9: Cross section view of the polarized target to be used by this experiment.

As part of the program to minimize the sources of systematic errors, the target polarization direction will be reversed after each annealing by adjusting the microwave frequency.

A 10% radiator will be mounted in front of the magnet sweeper system. Taking into account the size of the magnet and its downstream shielding, the distance between the radiator and the polarized target will be 2 m.

2.2 The Photon Detector

There is a substantial overlap between key participants in this experiment and the Neutral Particle Spectrometer (NPS) collaboration, who will build the NPS (see Ref. [36] for details about the NPS calorimeter) for this and other proposed experiments, for example, E12-13-010, E12-13-007 and unpolarized WACS experiments. The sensitive region of this calorimeter is 30 (horizontal) x 36 (vertical) inches, sitting on a frame allowing for easy movement. The position resolution of the NPS is 3 mm and the energy resolution, $\sigma_E/\sqrt{E}$, is better than 3%.

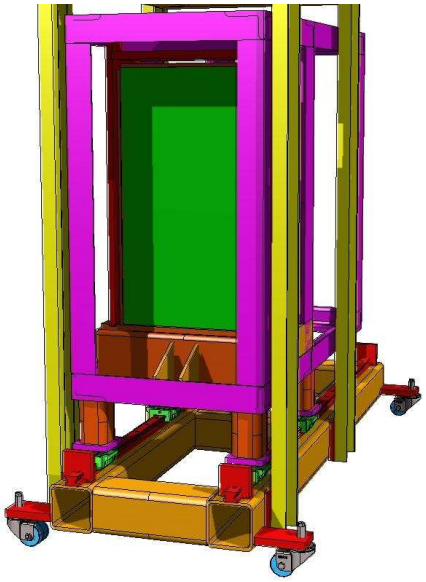

Figure 10: The front view of the Neutral Particle Spectrometer (NPS).

For this experiment the NPS will be placed at 28°, while the SBS will be positioned at 25°. The large SBS and NPS angular and momentum acceptances will allow binning of the experimental data into several s and t bins.

2.3 Proton Polarization in the Target

The target polarization will be measured via NMR to an accuracy of 4%. An independent measure of the target polarization can be obtained as follows: With the sweeper magnet turned off, the radiator removed, and the beam intensity lowered enough to protect the target, one can select elastic electron–proton scattering events. For elastic electron proton scattering, the beam–target asymmetry can be calculated from the following expression [33, 34]:

$$A^{ep} = \frac{2\sqrt{\tau(1+\tau)}\,\tan\frac{\theta}{2}}{g^2 + \tau\epsilon^{-1}} \cdot (g\,\sin\phi + \sqrt{\tau}\,\cos\phi) \tag{9}$$

where $g = G_E^p/G_M^p$ is the ratio of the proton form factors, θ is the scattering angle, $\tau = Q^2/4M_p^2$, (M_p is the proton mass), and $Q^2 = 4E_iE_f\sin^2\frac{\theta}{2}$, $E_{i(f)}$ is the initial (final) electron energy, $\epsilon^{-1} = 1 + 2(1+\tau)\tan^2\frac{\theta}{2}$ and $\sin\phi = \cos\frac{\theta}{2}/\sqrt{(1+E_i/M_p)(2+E_i/M_p)\sin^2\frac{\theta}{2}}$. This formula takes into account that the polarization axis is along the beam direction and in the scattering (horizontal) plane. Thus, the product of the beam and the target polarization will be determined with a statistical accuracy of 0.02. This will provide an additional (independent of the NMR measurement) monitor of the beam and target polarization.

3 Technical Considerations

A key new element of instrumentation in this experiment is the photon calorimeter, the Neutral Particle Spectrometer, proposed by the NPS collaboration [36]. An additional element is a deflection magnet as discussed in general terms in Sec. 2 and in detail below.

3.1 Untagged Bremsstrahlung Source

The experimental program laid out in this proposal requires a real photon source. At JLab only Halls B and D have built-in real photon capabilities, so one of the primary tasks of the collaboration is to design, simulate the performance, and build a clean photon source that can safely operate in Hall A.

The technical solution proposed is an untagged bremsstrahlung gamma source consisting of the following components:

- A thick (10% radiation length) radiator.
- A normal conducting magnet ("amagnet") providing a dipole field with a large enough $\int \vec{B}d\vec{l}$ to sweep primary beam electrons out of the beam line. While the footprint of the magnet itself would be 100x50x60 cm^3, in order to reduce the background radiation to an acceptable level an outer shielding (see below) made of iron blocks is needed. The proposed setup is shown in Figures 11 and 12.
- Enough radiation shielding both inside and in the surrounding area of the magnet to ensure that the radiation level at the Hall boundaries does not exceed allowable limits. This shielding effectively turns the magnet into a sweeper/mini beam dump combination.
- A magnet bore featuring a long (1 m) copper cylinder with small (2 mm) diameter holes drilled in it at increasingly larger distances from the center and at different azimuths, as shown in Fig. 12. This cylinder will be able to (slowly) rotate around its axis. In conjunction with a slow raster applied to the primary beam, this device will form a "mechanical raster" protecting the target from overheating/boiling.

To test the validity of the proposed setup, the whole assembly shown in Fig. 11 was simulated using Geant4. A magnetic (with a 2 cm mesh size) field map produced by TOSCA was imported into Geant4 and used in the Monte Carlo simulation. A 3D interpolation function was implemented/used in the code.

Figure 13 illustrates the effectiveness of the proposed magnet and shielding combination at containing both charged (red traces in the right panel) and neutral (green trajectories) particles.

Figure 14 shows the profile of the photon beam one meter downstream of the magnet. Only photons of energies above 6 GeV were selected. The red curve represents the outline of the 2 mm-hole in the central part of the magnet that was used in the simulation. The corresponding transverse momentum distribution for the photons shown in 14 is shown in Figure 15. To test the effectiveness of the central piece of the magnet the transverse size of

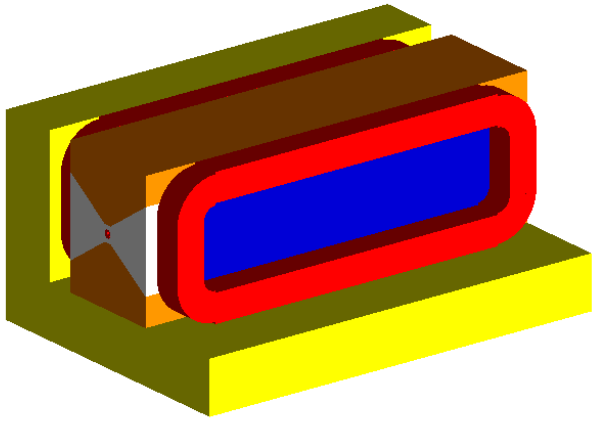

Figure 11: Schematic of the sweeper magnet. Half of the concrete shielding around the magnet (yellow) is shown. The 26" Fe shielding surrounding the whole assembly was removed for clarity. The central area of the magnet bore will be a copper cylinder with a spiral pattern of 2 mm diameter holes as shown in Figure 12. This assembly will act as a "mechanical raster"/collimator for the untagged bremsstrahlung gamma source.

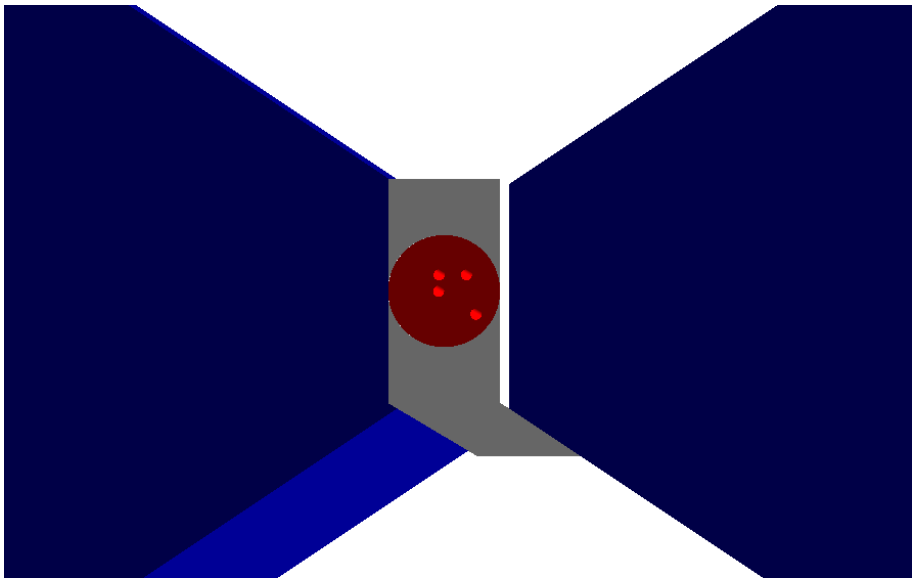

Figure 12: Central area of the magnet bore showing the spiral pattern of holes that will form the "mechanical raster" of the untagged bremsstrahlung gamma source. Both the gray and the red pieces extend the full length of the magnet. A pattern of four 2 mm diameter holes are seen in the cylindrical piece.

the primary electron beam used in this simulation was larger than the 2 mm diameter of the hole.

Figure 13: Simulation of a small (100 events) sample of electron interactions. The right panel shows the full shielded magnet setup while the left panel shows the same events without the magnet and shielding drawings.

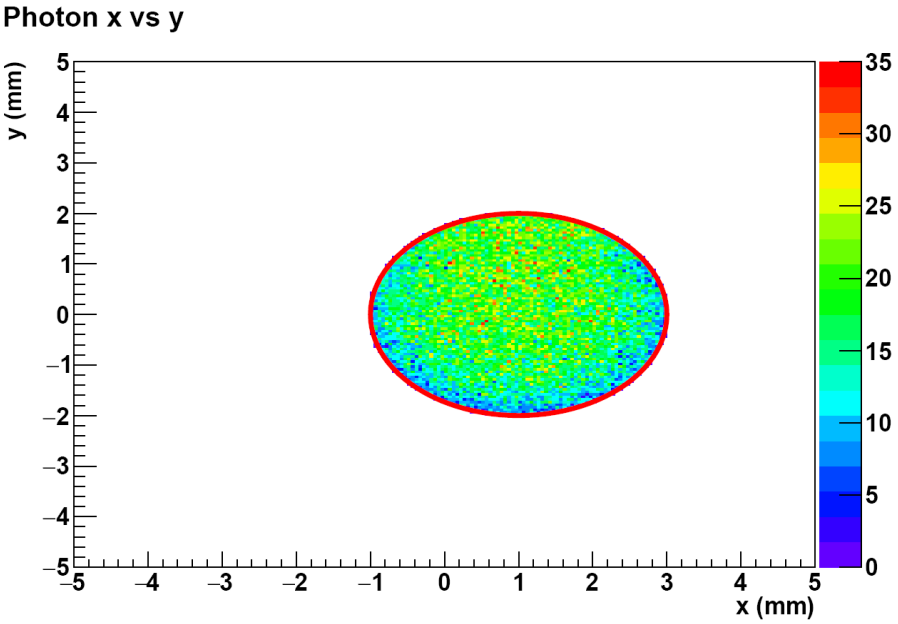

Figure 14: x vs y distribution of the bremsstrahlung photons of energies above 6 GeV, one meter downstream of the magnet. A 2mm- diameter hole through the center piece of the magnet was assumed for this particular simulation.

3.2 Projected Radiation Budget for the NPS and the Radiation Level in Hall A

As the sweeper magnet proposed here and its shielding effectively act as a (mini)beam dump keeping the dose escaping the magnet area at an acceptable level is of the utmost importance for this project. A realistic dose rate calculation was carried out, using the Geant4 simulation described above, as follows [37]:

"Ghost", vacuum-filled volumes were defined and positioned 15 m from the magnet (this is the typical distance at which radiation level is monitored) . The neutron flux through these volumes shown was monitored and for each neutron crossing one of the scoring volumes the Kinetic energy, weighted with and the path traveled in the scoring volume were accumulated and normalized to the volume of the ghost volume. Using this information one

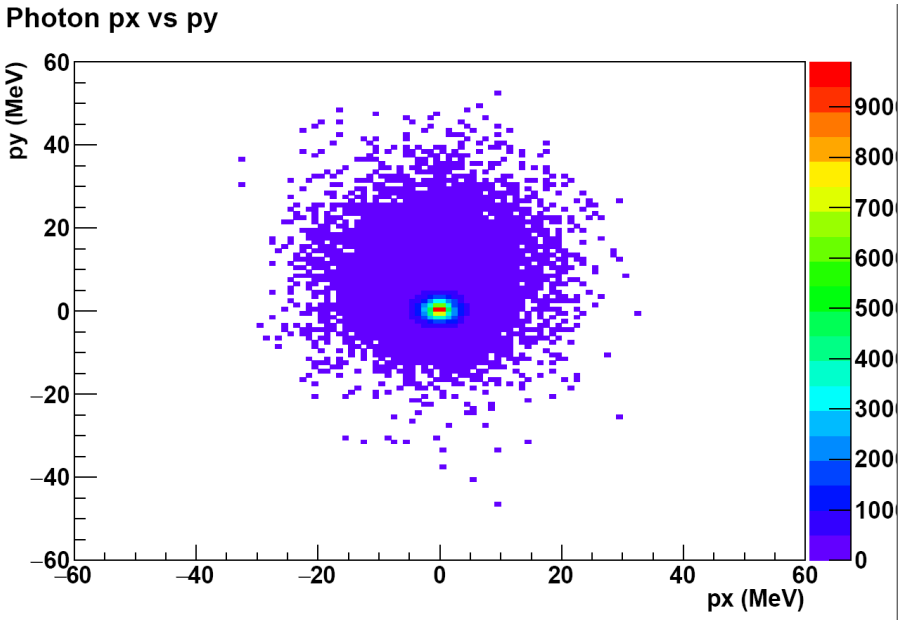

Figure 15: Transverse momentum distribution for the photons shown above.

can then use the standard provided in the US Code of Federal Regulations (CFR) Title 10 Part 835 Occupational Radiation Protection (which in turn follows closely the International Commission on Radiation Protection recommendations)[1] to convert the (weighted) neutron energy into a dose. To obtain a dose rate one needs to take into account the number of beam electrons per second in the real beam (i.e. "# wanted electrons/s")

$$\#\ wanted\ electrons/s = I/e \tag{10}$$

where I is the beam current (assume 8.8 GeV at 1.2 μA) and e is the electron charge, the actual number of electrons simulated (# simulated electrons), and the time:

$$DoseRate = dose(mrem) \times \frac{\#\ wanted\ electrons/s}{\#\ simulated\ electrons} \times 3600s \tag{11}$$

Figure 16 shows the neutron hit distribution for the six "ghost" volumes surrounding the magnet. For the six panels shown in 16 the dose rate estimates are (top to bottom and left-to-right): 24.4, 24.1, 220.5, 265.5, 24.1, and 23.4 mrem/hr. Other particle types (photons, charged particles) were monitored but, according to the simulation, will be contained by the sweeper magnet (except for the beam photons, of course) and/or its shielding and are not expected to make a significant contribution to the radiation budget.

[1]The Nuclear Regulatory Commission [38] uses almost the conversion tables.

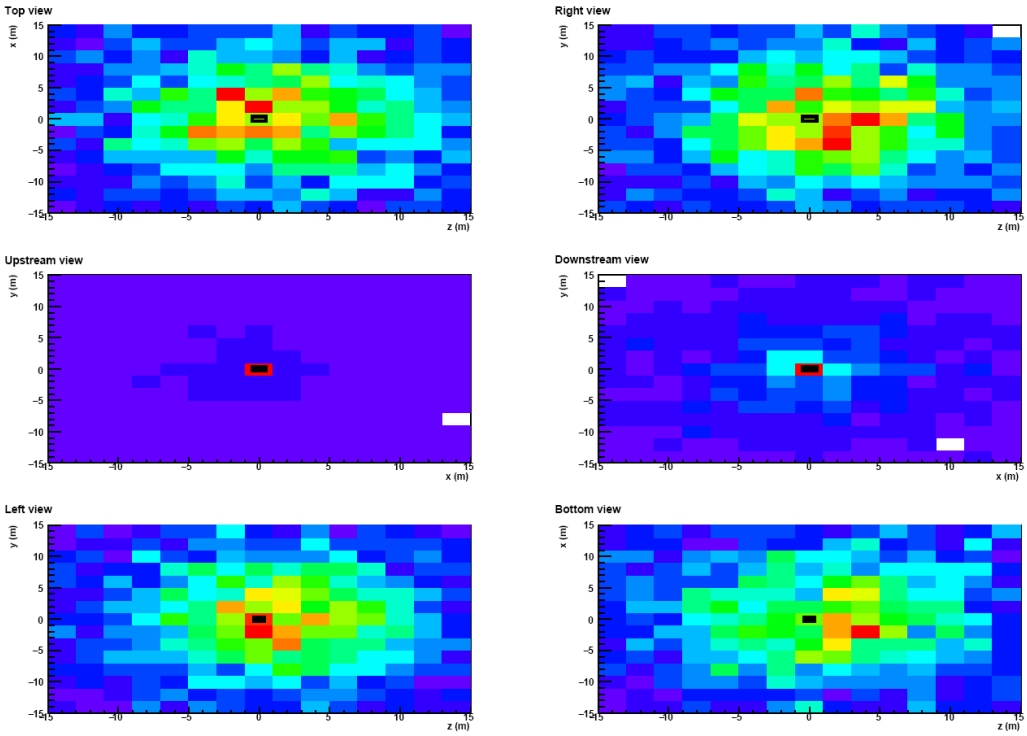

Figure 16: Neutron hit patterns for the six "ghost" volumes surrounding the magnet. For the six panels shown the dose rate estimates are (top to bottom and left-to-right): 24.4, 24.1, 220.5, 265.5, 24.1, and 23.4 mrem/hr.

4 Proposed Measurements

An 80% longitudinally polarized electron beam with a current of 1.20 μ A at energy of 8.8 GeV will be used in the proposed experiment. A 10% radiator, together with a shielded, normal conducting dipole magnet acting as a sweeper/beam dump combination will produce a narrow, untagged bremsstrahlung photon source. This photon beam will strike a 3 cm long NH_3 longitudinally polarized target.

The SBS spectrometer will detect the recoil proton, while the scattered photon will be detected by the Neutral Particle Spectrometer(NPS). The angle and distance from the target for each spectrometer were optimized via extensive (Geant4) simulation.

4.1 The Kinematics

This experiment will use the SBS and NPS spectrometers. The main parameters of these detectors are summarized in Table 1 and Table 2.

Angle	25°
Distance [cm]	371 (to detector) 160 (to magnet)
$\Delta\Omega$ [msr]	70
$\delta p/p$ [%]	$0.29 + 0.03p$ [GeV]
$\delta\theta$ [mrad]	$0.14 + 1.34/p$ [GeV]
$\delta\phi$ [mrad]	$0.09 + 0.59/p$ [GeV]

Table 1: SBS parameters.

Angle	28°
Distance [cm]	200
$\Delta\Omega$ [msr]	100
$\delta p/p$ [%]	$3/\sqrt{(E)}$ [GeV]
$\delta\theta$ [mrad]	3
$\delta\phi$ [mrad]	3

Table 2: NPS parameters (assume 60 cm x 70 cm profile).

The kinematic coverage for this proposal is shown in Fig. 17.

4.2 Backgrounds

Several processes that can constitute sources of physics background were considered:

A large background source for mixed electron-photon beam experiments are elastic electron-proton events where the electron radiates a photon either prior to or after the interaction

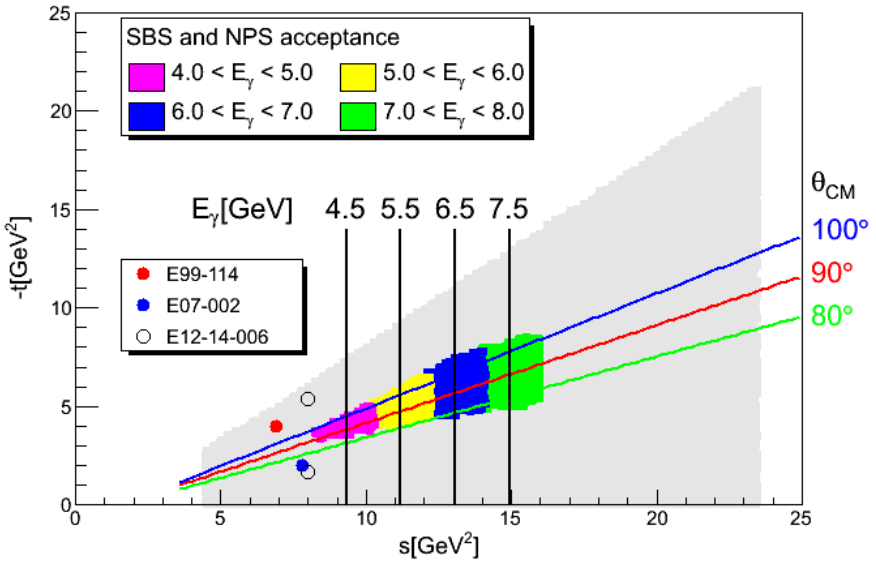

Figure 17: The kinematic coverage (Mandelstam variable t as a function of s) of this proposal taking into account the SBS (at 25°) and NPS (at 28°) acceptances. The vertical lines correspond to photon energies of 4.5, 5.5, 6.5, and 7.5 GeV. The diagonal lines correspond to 80, 90, and 100° cm angles. Results from previous JLab experiments (circle symbols) are also shown.

with the photon. The sweeper magnet/dump combination will ensure that no electrons interact with the polarized target. A co-planarity test between the detected photon and proton momenta should be able to veto any stray electrons that might get into the polarized target.

The primary background comes from neutral pion photo production from the protons in the target. It can be separated only on a statistical level by using the difference in the shapes of the distribution of WACS and H(γ, π^0) events.

This background leads to a large dilution factor, which affects the statistical accuracy of the measurements. The pion can also be produced from bound protons in nitrogen. Motion of the nucleons in nuclei, and FSI, reduce dramatically the dilution of WACS events. The nuclear pion process was investigated by using E99-114 data obtained from an aluminum target. We found that at conditions similar to those proposed here, pions produced from nuclei increase the dilution factor by less than 10%.

4.3 Production event rates

The event rates are the products of the luminosity, the cross section, and the acceptances of the detectors, as well all other factors such as DAQ dead time and detection efficiency. The rate, N_{WACS} can be calculated as:

$$N_{WACS} = \frac{d\sigma}{dt}_{WACS} \frac{(E_\gamma^f)^2}{\pi} \Delta\Omega_\gamma f_{\gamma p} N_p N_\gamma \qquad (12)$$

where $\frac{d\sigma}{dt}$ is the WACS cross section, the factor $\frac{(E_\gamma^f)^2}{\pi}$ is the Jacobian that converts dt to $dEd\Omega$, $\Delta\Omega_\gamma$ is the solid angle of the WACS events, $f_{\gamma p}$ is the NPS-SBS acceptance, N_γ is the number of incident photons per unit time, and N_p is the number of target protons.

E99-114 measured real Compton scattering cross section at four electron beam energies of 2.34, 3.48, 4.62, and 5.76 GeV and $\theta_p^{\rm cm}$ in the range of $60^\circ - 130^\circ$. Table 3 shows the results for the average photon energy of 4.3 GeV. Also shown in the table is the dilution factor D, which is defined as the ratio of total γ seen from the π^0 and Compton signal to the γ seen from the Compton signal alone: $D = (N_{\gamma,\pi^\circ} + N_{\gamma,\gamma})/N_{\gamma,\gamma}$ for the kinematically correlated photon-proton events.

kin. 4#	$\theta_\gamma^{\rm lab}$, degree	t, GeV^2	$\theta_p^{\rm cm}$, degree	D	$d\sigma/dt$, pb/(GeV/c)^2
4A	22	-2.03	63.6	2.13	496.
4B	26	-2.57	72.8	1.54	156.
4C	30	-3.09	81.1	1.67	72.
4D	35	-3.68	90.4	2.75	42.
4E	42	-4.39	101.5	2.80	29.
4F	50	-5.04	112.1	2.42	38.
4G	57	-5.48	119.9	2.83	46.
4H	66	-5.93	128.4	3.89	61.

Table 3: The WACS cross section at $s = 9$ GeV^2- 4 pass kinematics in E99-114.

According to the E99-114 results [35] the WACS cross-section could be presented with the following s and t dependancies:

$$\left.\frac{d\sigma}{dt}\right|_{s,t} = \left.\frac{d\sigma}{dt}\right|_{s_0,t_0} \cdot \left(\frac{s}{s_0}\right)^{3.5} \cdot \left(\frac{t}{t_0}\right)^{4.0} \tag{13}$$

We used the expression above to extrapolate the existing data from E99-114 [35] and calculate the WACS differential cross section for the projected kinematical points.

To determine the angular acceptance, we developed a Geant4 simulation program which included the target magnet coils, their magnetic field profile, and the geometry of NPS and SBS. The position of the two spectrometers was optimized for high s and t Wide–angle Compton scattering kinematics required in this proposal. The WACS events and π^0 backgrounds were simulated. The acceptance of WACS photons in a three dimensional space (Energy, θ, and ϕ), as well as the single arm acceptances for photons (NPS) and protons (SBS) were determined.

Table 4 shows the central values for the expected differential cross–section and the scattered photon energies for the four values of s this experiment will measure.

The number of proton nuclei in the target was computed using the formula:

$$N_p = \frac{Z}{A} t f_{pack} N_A \tag{14}$$

Kin	1	2	3	4
$s, [\mathrm{GeV}^2]$	9.4	11.0	13.0	15.0
$-t, [\mathrm{GeV}^2]$	4.0	4.9	5.8	6.5
$E'_\gamma, [\mathrm{GeV}]$	2.4	2.7	3.3	4.0
$d\sigma/dt, [\mathrm{cm}^2/\mathrm{GeV}^2]$	21×10^{-36}	5.3×10^{-36}	1.5×10^{-36}	0.6×10^{-36}

Table 4: Expected WACS cross–sections and scattered photon energies for the kinematics proposed in this experiment.

For the $g2p$ target the estimate is $N_p = 1.65 \times 10^{23}$ protons. Assuming a 1.2 μA beam intensity and a 10% radiator, the expected photon flux for the four s bins listed above is summarized in Table 5.

Kin	1	2	3	4
$E_\gamma, [\mathrm{GeV}]$	4-5	5-6	6-7	7-8
$N_\gamma, [\mathrm{s}^{-1}]$	1.5×10^{11}	1.2×10^{11}	1.1×10^{11}	0.9×10^{11}

Table 5: Expected photon flux and incident photon ranges for the four kinematics points proposed.

Figure 18 shows the Geant4 results for the acceptance of our experimental setup for the four kinematic points proposed. Single arm as well as the combined SBS–NPS acceptance is shown. For the four bins proposed, the $f_{\gamma p}$ factor is 0.21, 0.43, 0.49 and 0.45, respectively.

Based on the assumptions and simulations described above, the expected counting rate for the kinematic points proposed in this experiment is summarized in Tab. 6.

Kin	1	2	3	4
$s, [\mathrm{GeV}^2]$	9.4	11.0	13.0	15.0
$-t, [\mathrm{GeV}^2]$	4.0	4.9	5.8	6.5
E'_γ [GeV]	2.4	2.7	3.3	4.0
$d\sigma/dt, [\mathrm{cm}^2/\mathrm{GeV}^2]$	21×10^{-36}	5.3×10^{-36}	1.5×10^{-36}	0.6×10^{-36}
$f_{\gamma p}$	0.21	0.43	0.49	0.45
$N_\gamma, [\mathrm{s}^{-1}]$	1.5×10^{11}	1.2×10^{11}	1.1×10^{11}	0.9×10^{11}
N_{WACS}, (per hour)	72	36	18	7.2

Table 6: Expected WACS counting rates for the four kinematic points proposed.

4.4 Required Statistics

The statistics required for obtaining the specified accuracy of ΔA_{LL} can be calculated from

$$N_{WACS,required} = D/(P_\gamma P_p \Delta A_{LL})^2$$

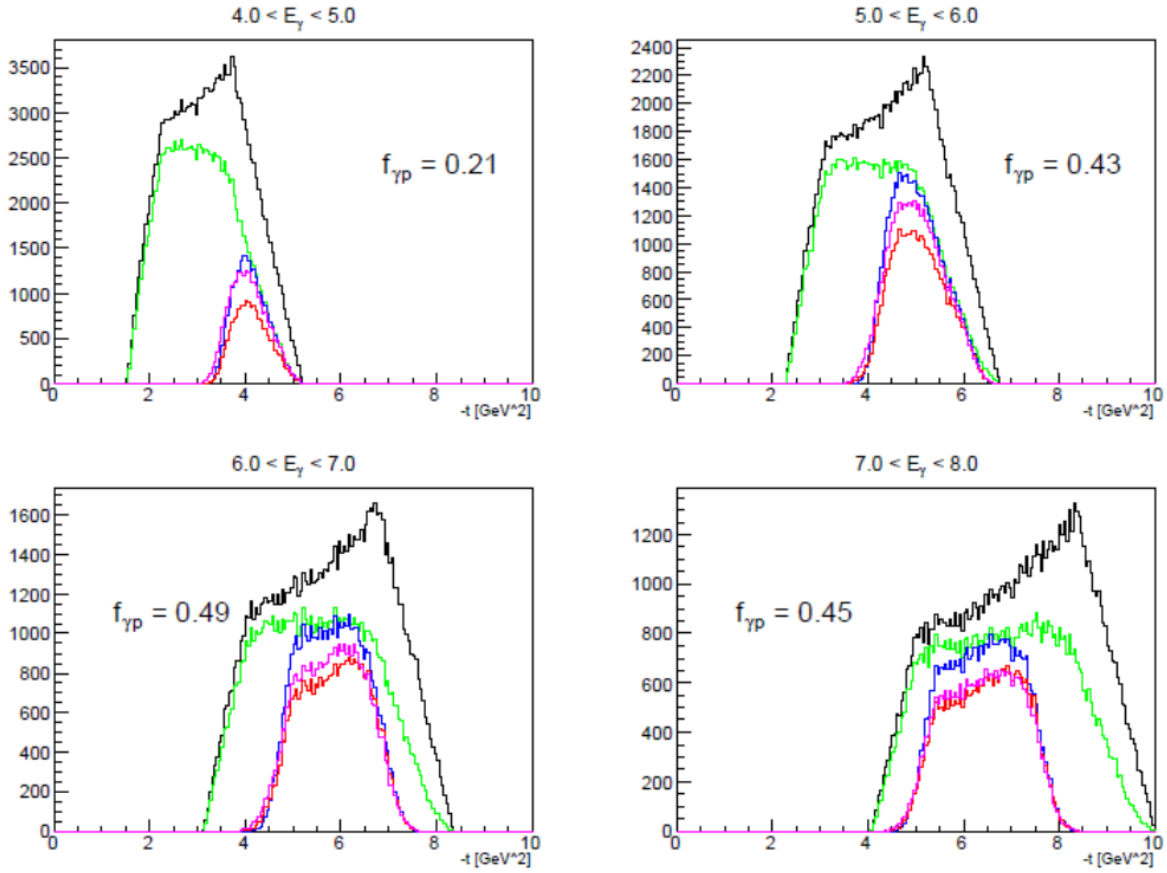

Figure 18: Monte Carlo simulation of the spectrometer acceptance for the four kinematic bins proposed. The NPS acceptance is shown in green, the SBS acceptance is shown in blue (no field) and red (with SBS and target fields), and the combined SBS–NPS acceptance is shown in purple. The available phase space is shown in black.

where N_{WACS} is the number of accumulated WACS events, P_γ is the photon beam polarization, $P_p = 0.75$ is the averaged proton polarization in the target, and D is the dilution factor. As extracted from Figure 19, the P_γ factor for the kinematic points of interest is 0.52, 0.63, 0.72 and 0.77, respectively.

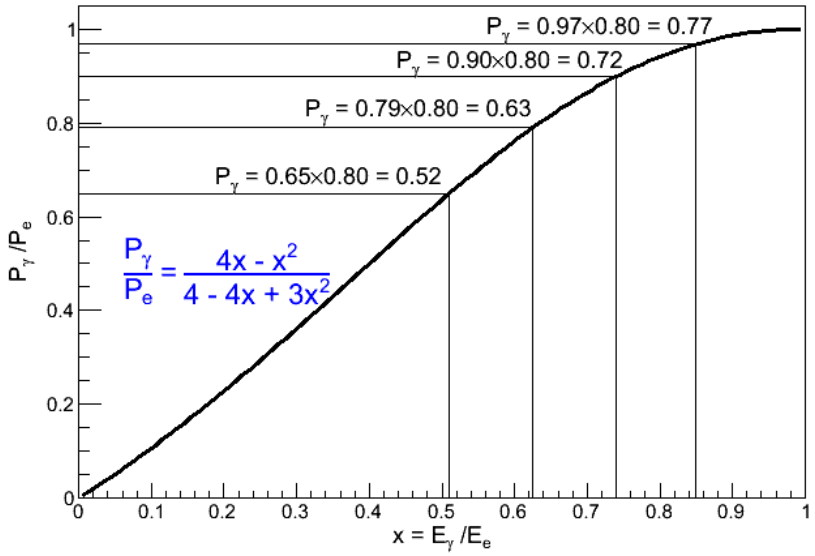

Figure 19: Ratio of the photon and electron polarizations as a function of their energies.

The dilution factor D quantifies the ratio between the total number of events recorded and the actual number of real–photon induced events. Figure 20 shows the simulated background subtraction for one of the s bins proposed. The dilution factor for all four s bins is 3.1, 3.8, 4.0 and 3.9, respectively.

Assuming a conservative 250 hours of production data, table 7 summarizes the expected ΔA_{LL} precision for all kinematic points. For all points, the absolute uncertainty is smaller than 0.09.

Kin	1	2	3	4
ΔA_{LL}	0.034	0.043	0.055	0.081

Table 7: Expected ΔA_{LL} statistical precision in the proposed experiment.

4.5 Systematic Uncertainty

In Table 8 we summarize the uncertainties expected to contribute to the systematic error of A_{LL}. As demonstrated in the E08-027/E08-007 experiment [39], the relative uncertainty in the target polarization can, through careful minimization, be driven down to about 3.9%.

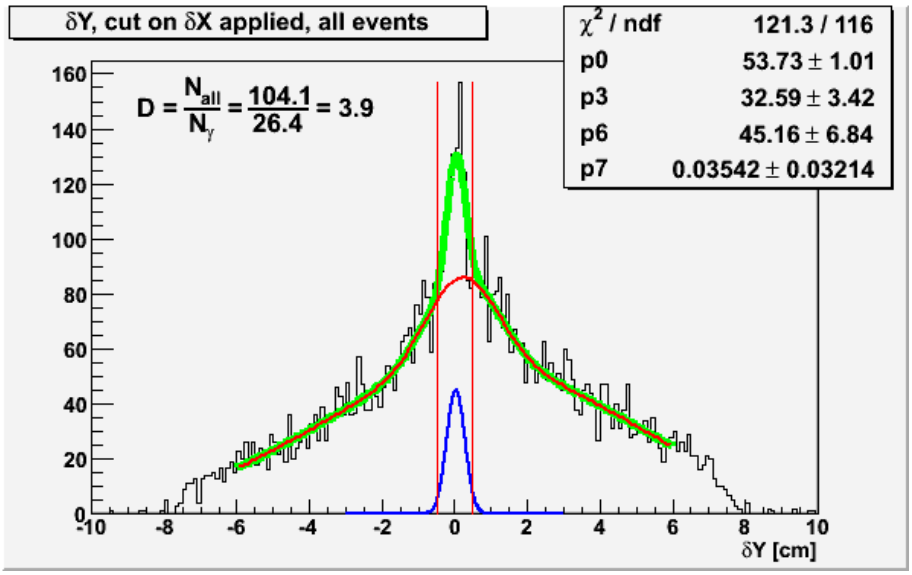

Figure 20: Subtraction of background events for one of the kinematics bins proposed and extraction of the dilution factor.

Assuming that the beam polarization will be known up to a 3% uncertainty, the total polarimetry uncertainty is expected to be about 5%. The uncertainty associated with the packing fraction of the ammonia in the target is expected to be at or below the level of 3%. These error sources are scale dependent contributions, i.e. they will have the same effect on all kinematic points.

Other parameters are less critical for the current "beam helicity" type experiment. The primary beam charge calibration uncertainty is expected to contribute about 1%. The uncertainties in detector resolution and efficiency are expected to contribute at the level of 2%. The combined trigger and tracking efficiency error contribution is estimated to be below 2%. The SBS–NPS acceptance uncertainty is expected to contribute at the level below 2%. The largest point-to-point uncertainty source is associated with the signal extraction.

Uncertainty Source	Systematic [%]
Polarimetry	5.0
Packing fraction	3.0
Charge Determination	1.0
Trigger/Tracking efficiency	2.0
Acceptance	2.0
Detector resolution and efficiency	2.0
Background subtraction	4.0
Total	8

Table 8: Estimates of the systematic uncertainty contributions to the systematic error of A_{LL}.

Adding in quadrature all the (independent) uncertainty sources listed above, the total systematic uncertainty for this experiment is expected to be about 8%. As the error budget is clearly dominated by polarimetry and background subtraction, time–dependent drifts in these quantities must be kept under control.

5 Expected Results and Beam Time Request

5.1 Expected Results

The purpose of this experiment is to measure the initial state helicity correlation asymmetry A_{LL} with a precision sufficient to obtain conclusive evidence on the dominance of the specific reaction mechanism. We propose to obtain the statistical precision for A_{LL}, given in Table 7 and shown in Fig. 21. Using the handbag formalism to interpret the results of the A_{LL} and A_{LT} we plan and calculate the values for the form factor ratio R_A/R_V. The data will also be used to determine of the polarization parameters in the single-pion photoproduction.

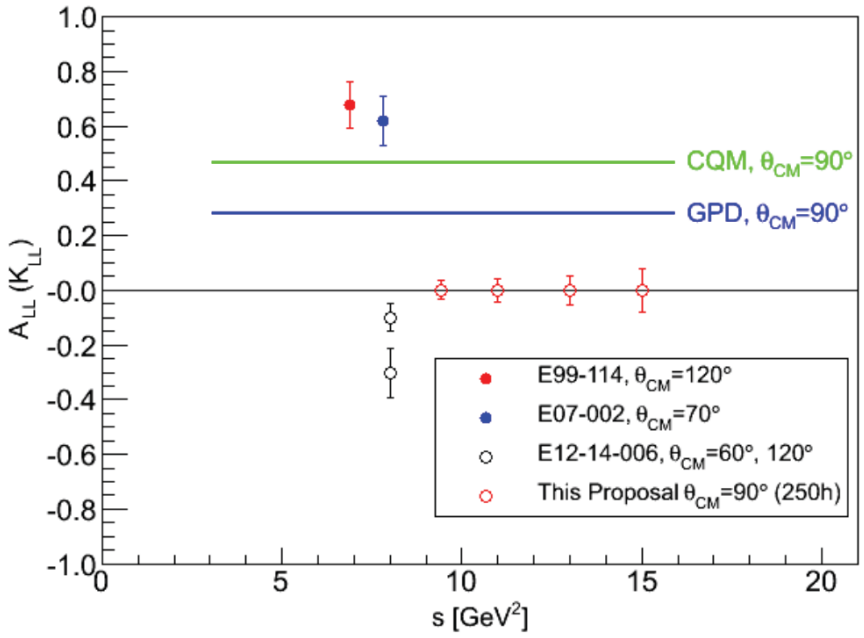

Figure 21: A_{LL} as a function of s showing the projected impact (error bars and range) of the proposed measurement (open red circles).

5.2 Beam Time Request

The proposed experiment will use a polarized electron beam of energy 8.8 GeV with currents of 1.2 μA. The requested beam time is summarized in Table 9.

We will need eight hours to calibrate the calorimeter with $e-p$ elastic coincident events. The radiator will be out of the beam line during this procedure. To measure the packing fraction of the material in the target cell, we are requesting 24 hours in total to do an empty cell and carbon target measurements. We plan to measure the beam polarization with the Möller polarimetry twice. It will take about four hours for each measurement.

Also shown in Table 9 is a summary of the time required for configuration changes. It will take less than four hours to perform each annealling of the target in order to restore the

Purpose	Description	Time Hours
NPS/SBS calibration	$e-p$ elastic	24
Photon beam commissioning		16
Packing fraction	Empty cell and C target	24
Beam polarization (x2)	Möller polarimetry	8
Target annealing	4 hours each	8
Target polarization		20
Total overhead time		100
WACS data production	A_{LL}	250
Total requested time		350

Table 9: Beam time request for this experiment.

optimal target polarization. We will need to anneal the target every 4-5 days at projected radiation intensity. We estimate 20 hours committed to target polarization calibrations. We estimate 100 hours of all overhead items listed above. The total time requested is a combination of the required beam time and the overhead time.

The total request is 350 hours, or 15 days.

6 Summary

We request 350 hours of beam time to measure the initial state helicity correlation asymmetry A_{LL} in Wide-angle Compton Scattering (WACS) with an accuracy of 0.09 by scattering circularly polarized photons from a longitudinally polarized proton target at invariant s in the range of 8 to 16 GeV^2 for four scattering angles between $\theta_p^{\rm cm} = 80^\circ$ and $\theta_p^{\rm cm} = 100^\circ$. The experiment will use an 8.8 GeV, 1.2 μA, 80% polarized electron beam and a $g2p$ longitudinally polarized target. A sweeper–dump magnet combination will be used to produce a narrow photon beam. The scattered photons will be detected by the NPS spectrometer while the SBS spectrometer will detect protons.

The proposed experiment has a large FOM of the proposed experiment (compared with known WACS experiments) and will carry out its measurements at large s and t in the wide–angle regime. These are optimal conditions for unambiguously testing the applicability regime of GPDs and will most likely resolve the (apparent) puzzles discovered by recent Hall A and Hall C experiments.

Knowledge of the initial state helicity correlation asymmetry A_{LL} in WACS at these kinematics will allow a rigorous test of the reaction mechanism for exclusive reactions at high t, which is crucial for the understanding of nucleon structure. This measurement should increase the experimental confidence in the applicability of the GPD approach (and its limitations) to real–photon induced reactions, paving the way for many other real–photon based studies such as pion production, deuteron photodisintegration, thus playing a major role in the nucleon structure physics program at JLab.

References

[1] D. Müller *et al.*, *Fortschr. Phys.* **42**, 101 (1994); X.D. Ji, *Phys. Rev. Lett.* **78**, 610 (1997); A.V. Radyushkin, *Phys. Rev.* **D 56**, 5524 (1997).

[2] A.V. Belitsky and A.V. Radyushkin, *Phys. Rep.* **418** 1 (2005).

[3] G. R. Farrar and H. Zhang, *Phys. Rev. Lett.* **65**, 1721 (1990), *Phys. Rev.* **D 42**, 3348 (1990).

[4] A.S. Kronfeld and B. Nizic, *Phys. Rev.* **D 44**, 3445 (1991); M. Vanderhaeghen, P.A. M. Guichon and J. Van de Wiele, *Nucl. Phys.* **A 622**, 144c (1997); T. Brooks and L. Dixon, *Phys. Rev.* **D 62** 114021 (2000).

[5] A.V. Radyushkin, *Phys. Rev.* **D 58**, 114008 (1998).

[6] M. Diehl, T. Feldmann, R. Jakob, P. Kroll, *Eur. Phys. J.* **C 8**, 409 (1999).

[7] H. W. Huang, P. Kroll, T. Morii, *Eur. Phys. J.* **C 23**, 301 (2002), *Erratum ibid.*, **C 31**, 279 (2003); H. W. Huang, private communication.

[8] G.A. Miller, *Phys. Rev.* **C 69**, 052201(R) (2004).

[9] F. Cano and J. M. Laget, Phys. Lett.**B 551** 317 (2003); Erratum-ibid.**B 571**:260, (2003).

[10] N. Kivel and M. Vanderhaeghen, *Journal of High Energy Physics* **4**, 1 (2013); *Nucl. Phys.* **B 883**, 224 (2014); hep-ph/1504.00991 (2015).

[11] S.J. Brodsky and G. Farrar, *Phys. Rev. Lett.* **31**, 1153 (1973).

[12] M.A. Shupe *et al.*, *Phys. Rev.* **D 19**, 1921 (1979).

[13] A. Danagoulian *et al.*, *Phys. Rev. Lett.* **98**, 152001 (2007).

[14] D. J. Hamilton *et al.*, *Phys. Rev. Lett.* **94**, 242001 (2005).

[15] N. Kivel and M. Vanderhaeghen, "QCD radiative corrections to the soft spectator contribution in the wide angle Compton scattering," arXiv:1312.5456 [hep-ph].

[16] N. Kivel, M. Vanderhaeghen, arXiv:1504.00991

[17] G. P. Lepage and S. J. Brodsky, *Phys. Rev.* **D 22**, 2157 (1980).

[18] A. Radyushkin, arXive:hep-ph/0410276 and Dubna preprint JINR P2 10717.

[19] T. Brooks and L. Dixon, *Phys. Rev.* **D 62** 114021 (2000)

[20] V.A. Matveev, R.M. Muradyan, and A.V. Tavkheldize, *Lett. Nuovo Cimento* **7**, 719 (1973).

[21] C. Bourrely, J. Soffer, Eur. Phys. J. **C 36** 371 (2004)

[22] M. Jones *et al.*, *Phys. Rev. Lett.* **84**, 1398 (2000).

[23] O. Gayou *et al.*, *Phys. Rev. Lett.* **88**, 092301 (2002).

[24] A. Puckett *et al.*, *Phys. Rev. Lett.* **104**, 242301 (2010).

[25] K. Wijesooriya *et al.*, *Phys. Rev. C* **66**, 034614 (2002).

[26] X. Ji, *Phys. Rev.* **D 55**, 7114 (1997), *Phys. Rev. Lett.* **78**, 610 (1997).

[27] A.V. Radyushkin, *Phys. Lett.* **B 380**, 417 (1996),

[28] M. Diehl, T. Feldmann, R. Jakob and P. Kroll, *Eur. Phys. J.* **C 39**, 1 (2005), arXiv:hep-ph/0408173.

[29] M. Diehl, P. Kroll, *Eur. Phys. J.* **C 73**, 2397 (2013), arXiv:1302.4604.

[30] G. A. Miller, *Phys. Rev.* **C 66**, 032201 (2002).

[31] M. Diehl, T. Feldmann, H. W. Huang and P. Kroll, *Phys. Rev.* **D 67**, 037502 (2003), arXiv:hep-ph/0212138.

[32] J. Pierce *et al.*, "Dynamically polarized target for the g2p and GEp experiments at Jefferson Lab", arXiv:1305.3295

[33] N. Dombey, Rev. Mod. Phys. 41, 236 (1969).

[34] T.W. Donnelly and A.S. Raskin, Ann. Phys. (New York) 169, 247 (1986); 191, 81 (1989).

[35] A. Danagoulian *et al.*, Phys. Rev. Lett, 98, 152001 (2007).

[36] `http://www.vsl.cua.edu/cua_phy/index.php/MainPage:Nuclear:NPS`

[37] Pavel Degtiarenko, private communication; also see http://lss.fnal.gov/archive/2008/pub/fermilab-pub-08-244-esh.pdf

[38] U.S. Nuclear Regulatory Commision: http://www.nrc.gov/reading-rm/doc-collections/cfr/part020/part020-1004.html

[39] D. Keller, Nucl. Inst. and Meth. A 728 133-144 (2013)